Geologic mapping of the Comet 67P/Churyumov–Gerasimenko's Northern hemisphere

L. Giacomini,[1]★ M. Massironi,[1] M. R. El-Maarry,[2] L. Penasa,[3] M. Pajola,[4]
N. Thomas,[2] S. C. Lowry,[5] C. Barbieri,[6] G. Cremonese,[7] F. Ferri,[3] G. Naletto,[8]
I. Bertini,[3] F. La Forgia,[6] M. Lazzarin,[6] F. Marzari,[6] H. Sierks,[9] P. L. Lamy,[10]
R. Rodrigo,[11,12] H. Rickman,[13,14] D. Koschny,[15] H. U. Keller,[16] J. Agarwal,[9]
M. F. A'Hearn,[17] A.-T. Auger,[10] M. A. Barucci,[18] J.-L. Bertaux,[19] S. Besse,[15]
D. Bodewits,[17] V. Da Deppo,[20] B. Davidsson,[14] M. De Cecco,[21] S. Debei,[22]
S. Fornasier,[18,23] M. Fulle,[24] O. Groussin,[10] P. J. Gutierrez,[25] C. Güttler,[9]
S. F. Hviid,[26] W.-H. Ip,[27] L. Jorda,[10] J. Knollenberg,[26] G. Kovacs,[9] J.-R. Kramm,[9]
E. Kührt,[26] M. Küppers,[28] L. M. Lara,[25] J. J. Lopez Moreno,[25] S. Magrin,[6]
H. Michalik,[29] N. Oklay,[9] A. Pommerol,[2] F. Preusker,[26] F. Scholten,[26]
C. Tubiana[9] and J.-B. Vincent[9]

Affiliations are listed at the end of the paper

ABSTRACT

The Optical, Spectroscopic, and Infrared Remote Imaging System (OSIRIS), the scientific imaging system onboard the *Rosetta* mission, has been acquiring images of the nucleus of the comet 67P/Churyumov–Gerasimenko since 2014 August with a resolution which allows a detailed analysis of its surface. Indeed, data reveal a complex surface morphology which is likely the expression of different processes which occurred at different times on the cometary nucleus. In order to characterize these different morphologies and better understand their distribution, we performed a geologic mapping of comet's 67P Northern hemisphere in which features have been distinguished based on their morphological, textural and stratigraphic characteristics. For this purpose, we used narrow-angle camera images acquired in 2014 August and September with a spatial scale ranging from 1.2 to 2.4 m pixel^{-1}. Several different geologic units have been identified on the basis of their different surface textures, granulometry and morphology. Some of these units are distinctive and localized, whereas others are more common and distributed all over the Northern hemisphere. Moreover, different types of linear features have been distinguished on the basis of their morphology. Some of these lineaments have never been observed before on a comet and can offer important clues on the internal structures of the nucleus itself. The geologic mapping results presented here will allow us to better understand the processes which affected the nucleus' surface and thus the origin and evolutionary history of comet 67P/Churyumov–Gerasimenko.

Key words: methods: observational – comets: general – comets: individual: 67P/ Churyumov–Gerasimenko.

1 INTRODUCTION

Rosetta, the European Space Agency mission, encountered the Jupiter family comet 67P/Churyumov–Gerasimenko on 2014 August 6. During the approach phase of the cruise, OSIRIS (The Optical, Spectroscopic, and Infrared Remote Imaging System; Keller et al. 2007) acquired images of the primary target, progressively revealing the complex morphology of the cometary nucleus. The first images acquired showed a dark (geometric albedo of 5.9 per cent at 550 nm; Sierks et al. 2015) bi-lobed comet, with a larger lobe, hereafter 'body', with dimensions of

★ E-mail: lorenza.giacomini@unipd.it
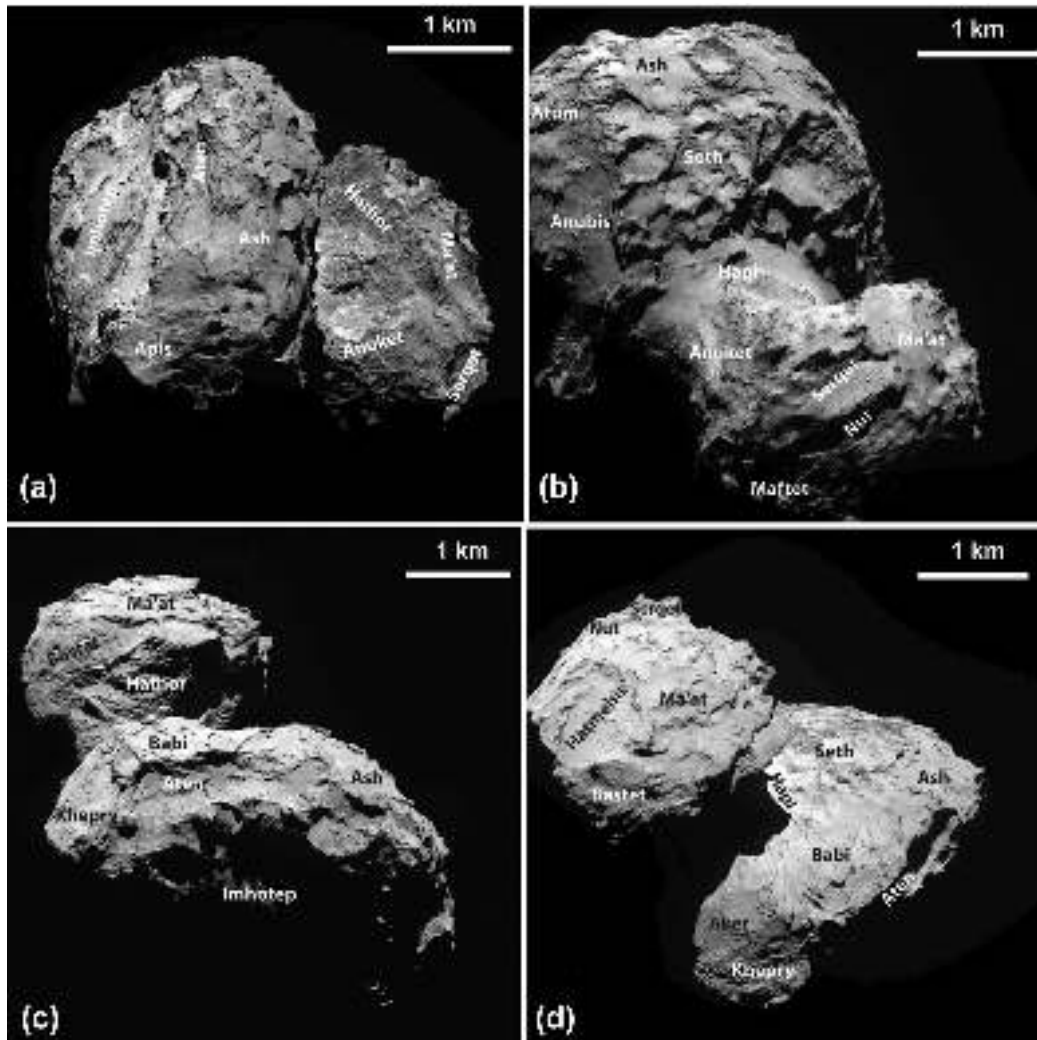
Figure 1. Four views of Comet 67P/Churyumov–Gerasimenko showing most of the Northern hemisphere of the nucleus. The physiographic region names described by El-Maarry et al. (2015a) are shown.

4.10 km × 3.52 km × 1.63 km, and a smaller lobe, hereafter 'head', with a size of 2.50 km × 2.14 km × 1.64 km (Jorda et al. 2016). The lobes are connected by a narrower region, hereafter 'neck'. When the distance from the comet became progressively smaller, OSIRIS images began to reveal a wide range of surface features (Fig. 1), suggesting a complex history for this body and allowing for an unprecedented detailed study of a comet surface (Thomas et al. 2015a).

Rosetta represented the latest of several missions designed to more closely study the nucleus of comets and better understand their nature. *Deep Space 1* reached the comet 19P/Borrelly in 2001 and returned images with a maximum spatial scale of 47 m pixel^{-1}. This scale factor allowed the detection of different types of terrains on the basis of topography, morphology and albedo which were classified as dark spots, mottled terrain, mesas and smooth terrain (Britt et al. 2004). Features such as ridges, troughs, pits and hills have also been detected. Terrain units and features have been interpreted to be the different expressions of erosion by sublimation (Britt et al. 2004).

Stardust flew by comet 81P/Wild 2 in 2004 January acquiring images with a maximum spatial scale of 14 m pixel^{-1} of the nucleus, showing a body heavily affected both by circular and irregular depressions (Brownlee et al. 2004). Circular features are thought to be the result of impact craters whereas the more irregular depressed regions could be formed by sublimation processes. The surface of Wild 2 appears affected by a large number of depressions and mesas which have been interpreted to be the remnants of oldest not sublimated terrains (Brownlee et al. 2004).

Finally, *Deep Impact* encountered comet 9P/Tempel 1 in 2005 and comet 103P/Hartley 2 in 2010, during its extended mission phase, named EPOXI (Extrasolar Planet Observation and Deep Impact Extended Investigation). Tempel 1 was imaged with a spatial scale less than 10 m pixel^{-1}, and, in small areas, less than 1 m pixel^{-1} (A'Hearn et al. 2005). This higher scale factor revealed different features and terrains. Several circular depressions were detected, both rimless and rimmed, some of which have been interpreted as impact crater remnants (Thomas et al. 2007). Moreover, other types of terrains were identified, such as smooth terrains and scarped pitted terrains, but more significantly, for the first time, layer structures were detected on a comet nucleus surface (Thomas et al. 2007) with important implications on the knowledge of the origin and evolution of a cometary body.

Hartley 2 was observed with a maximum practical mapping scale of 12 m pixel^{-1} (A'Hearn et al. 2011). Similar to 67P, Hartley
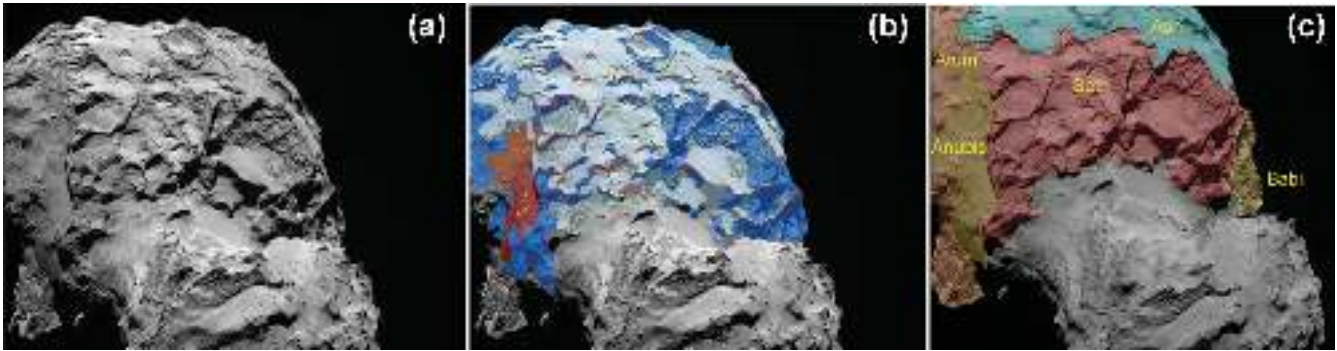
Figure 2. (a) NAC image showing part of the 67P's 'body'. Comparison between the corresponding (b) geological map and (c) regional physiographic classification (after El-Maarry et al. 2015a). In geological maps, both lineaments and surface are classified on the basis of their morphologies, surface textures, granulometry and source of origin. In regional classification, topographic boundaries and overall morphological similarities are instead considered.

2 is characterized by two lobes connected by a smoother region, referred to as the 'waist'. The most prominent features detected on the surface were bright mounds located on both lobes which could be linked to jet activity. In comparison, the 'waist' region is almost free of features. Finally, smooth, darker regions have been distinguished on the larger lobe which suggests the involvement of a depositional process (Thomas et al. 2013).

The detection of such morphological diversity on cometary surfaces permitted the performing of geomorphological mapping, which highlighted the major morphological units observed on the surface. However, due to limited spatial resolution of the available images, the geomorphological mapping of cometary nuclei allowed a few of the main physiographic regions to be detected.

On the contrary, OSIRIS image spatial resolution and coverage allow for the study of the morphology of 67P's surface in unprecedented detail. This includes the identification of major physiographic regions, described by El-Maarry et al. (2015a), as well as detailed geomorphological characterization essential for geologic mapping.

In this work, we present the first high-resolution geologic mapping of comet 67P/Churyumov–Gerasimenko's Northern hemisphere. About 70 per cent of the cometary nucleus surface, corresponding to the illuminated area during the 2014 August–September period, has been mapped. The remaining 30 per cent corresponds to the Southern hemisphere regions (unlit at the time considered in this work), whose geological maps have been performed by Lee et al. (2016). The mapping of the two hemispheres has been performed following the same classification criteria. The overlapping areas between the two hemispheres were matched and integrated with each other in order to create a uniform geological map of the entire surface.

The geologic mapping presented in this work classifies both surfaces and linear features on 67P's surface. Any geological map of a body's surface will incorporate distinct geological units. Each unit will have peculiar characteristics which distinguish it from all other units (Tanaka, Skinner & Hare 2011). In this work, a geologic unit identifies the surfaces which are characterized by similar texture and morphology, stratigraphic position, and possibly source region. Hence, a geologic map is different from a regional physiographic classification which classifies regions of the surface on the basis of prominent topographic boundaries and overall morphological similarities (e.g. El-Maarry et al. 2015a for 67P). In other words, regions are geomorphologic locations including several geologic units with distinct stratigraphic positions and textures which can be even equal among different regions. Therefore, in several cases

regional boundaries do not correspond to the geologic ones. Hence, regional classification and geologic mapping are complementary (see Fig. 2). The physiographic classification of 67P nucleus has already been presented by El-Maarry et al. (2015a) where 19 different regions have been defined in the Northern hemisphere, whose names will be used in this work, when needed, as geographic reference.

2 DATA AND METHODS

Geologic mapping of 67P's Northern hemisphere was performed using images provided by *Rosetta*/OSIRIS. This instrument is equipped with a narrow-angle camera (NAC), with 12 filters covering the spectral range of 250–1000 nm, and a wide-angle camera, with a combination of 14 filters in the spectral range of 240–720 nm (Keller et al. 2007). In this work, several OSIRIS NAC images with different illumination conditions and viewing angles have been analysed to define the different features and define their boundaries. The final mapping products have been shown in seven NAC images (Table 1), radiometrically calibrated (Tubiana et al. 2015) in orange filter (centred at 649 nm).

In particular, for the body we selected two NAC images acquired on 2014 August 5 and 6, when the spacecraft distance from the nucleus was about 130 and 116 km, respectively, and the corresponding spatial scales were 2.4 and 2.2 m pixel^{-1}. For the head, we used two NAC images acquired on 2014 August 5 and 7 when the distance was 122 and 81 km and the spatial resolution was 2.3 and 1.5 m pixel^{-1}, respectively. For the neck, we chose three NAC images acquired on 2014 August 20 and on 2014 September 2 and 3. These are the first images to include observations of the neck at emission angles most suitable for geological mapping. During this time, the distance from the comet decreased from about 86 to 64 km; therefore, the resulting image spatial scales were 1.6 and 1.2 m pixel^{-1}. To perform the geologic mapping, NAC images were imported into ArcGIS environment, and then geologic units and features were digitized as vector shapefiles.

Several geologic units have been identified on 67P's surface: (i) fine particle deposits, (ii) outcropping consolidated terrain, (iii) smooth terrain and (iv) mass wasting deposits. We classified as fine particle deposits all the areas covered by a fine material and characterized by a hummocky surface (Fig. 3a). At the spatial resolution of the considered OSIRIS, images appear similar to dust. However, on ROLIS data, one of the imaging systems mounted on Philae lander, these deposits show a granular aspect, down to centimetre size (Mottola et al. 2015; Pajola et al. 2016b). Outcropping consolidated terrain identifies the areas free of coating where

Table 1. List of OSIRIS NAC images used in this work.

Figure		Image ID
Fig. 1	(a)	NAC_2014-08-06T06.20.00.104Z_ID10_1397549100_F28
	(b)	NAC_2014-08-06T03.20.22.793Z_ID10_1397549200_F71
	(c)	NAC_2014-08-05T20.43.14.578Z_ID10_1397549300_F22
	(d)	NAC_2014-08-05T23.19.48.261Z_ID10_1397549100_F27
Fig. 2	(a), (b)	NAC_2014-08-06T02.43.16.574Z_ID30_1397549100_F22
	(c)	NAC_2014-08-16T10.59.16.348Z_ID30_1397549700_F22
Fig. 3	(a)	NAC_2014-10-04T17.00.31.652Z_ID10_1397549500_F22
	(b)	NAC_2014-09-21T01.09.01.354Z_ID10_1397549300_F22
	(c)	NAC_2014-09-17T03.10.13.767Z_ID10_1397549000_F24
	(d)	NAC_2014-09-14T01.20.50.325Z_ID10_1397549800_F22
	(e)	NAC_2014-10-02T12.11.26.599Z_ID10_1397549700_F22
	(f)	NAC_2014-09-14T16.56.07.330Z_ID10_1397549100_F22
Fig. 5	(a)	NAC_2014-08-16T15.59.14.568Z_ID10_1397549500_F22
	(b)	NAC_2014-10-04T18.44.22.560Z_ID10_1397549900_F22
	(c)	NAC_2014-09-19T15.09.52.414Z_ID10_1397549001_F41
	(d)	NAC_2014-09-19T16.27.13.346Z_ID10_1397549000_F16
Fig. 6	(a), (b)	NAC_2014-08-16T15.59.14.568Z_ID10_1397549500_F22
Fig. 7	(a), (b)	NAC_2014-08-06T02.43.16.574Z_ID30_1397549100_F22
Fig. 8	(a)	NAC_2014-09-11T18.34.00.439Z_ID10_1397549200_F22
	(b)	NAC_2014-09-16T04.26.01.334Z_ID10_1397549001_F41
Fig. 9	(a), (b)	NAC_2014-09-21T01.09.13.319Z_ID10_1397549000_F16
Fig. 10		NAC_2014-08-08T04.37.34.583Z_ID10_1397549300_F22
Fig. 11	(a), (b)	NAC_2014-08-07T21.20.34.586Z_ID10_1397549700_F22
Fig. 12	(a), (b)	NAC_2014-08-05T23.43.16.579Z_ID30_1397549000_F22
Fig. 13	(a)	NAC_2014-09-13T17.17.07.856Z_ID10_1397549001_F41
	(b)	NAC_2014-09-13T08.19.08.366Z_ID10_1397549800_F22
Fig. 14	(a)	NAC_2014-09-19T12.04.13.330Z_ID10_1397549000_F22
	(b)	NAC_2014-10-19T12.22.15.525Z_ID10_1397549600_F22
Fig. 15		NAC_2014-08-16T16.59.14.570Z_ID10_1397549400_F22
Fig. 16	(a), (b)	NAC_2014-08-20T01.42.54.569Z_ID30_1397549300_F22
	(c), (d)	NAC_2014-09-02T23.44.22.550Z_ID10_1397549500_F22
	(e), (f)	NAC_2014-09-03T06.44.22.578Z_ID10_1397549400_F22
Fig. 17	(a)	NAC_2014-09-19T02.34.29.049Z_ID10_1397549001_F23
	(b)	NAC_2014-09-12T18.50.47.875Z_ID30_1397549000_F16

a more consolidated terrain is exposed. This material shows a rocky appearance and likely identifies the terrain constituting the bulk of the nucleus (Fig. 3b). Smooth terrain shows a surface with no asperities or roughness, with a surface texture smoother than that of fine particle deposits (Fig. 3c). Although this terrain appears uniform at a scale of metres per pixel, it shows a granular aspect on images of about 0.34 m pixel^{-1} (Auger et al. 2015). Finally, mass wasting deposits include the deposits constituted by incoherent material located at the foot of steep walls (see Figs 2d–f).

To assess the origin of these deposits, we computed gravitational slopes for all the triangles of the three-dimensional 'SHAP7' model of the comet nucleus described by Jorda et al. (2016) using the method by Werner & Scheeres (1996) and a constant density of 532 kg m^{-3} (Jorda et al. 2016). Centrifugal acceleration for a rotational period of 12.4043 h (Mottola et al. 2014) was also computed and summed to the gravitational acceleration to estimate the local acceleration. The gravitational slopes (Fig. 4) were then computed as the angles formed by the local surface normal and the local acceleration (Jorda et al. 2012).

Comparing the gravitational slope maps with the position of where these deposits are located, it is clear that the mass wasting deposits are placed at the bottom of the areas with the higher gravitational slopes (corresponding to the steep walls; Fig. 4). Therefore, the mass wasting deposits are thought to have been formed by the gravitational collapse of cliffs, in accordance with Groussin et al. (2015a) and Vincent et al. (2016).

Mass wasting deposits show different surface textures, morphologies and placement. Therefore, we adopted a further classification for this unit, where the granulometry and the source region have also been taken into consideration. In accordance with this classification, we have identified three different subunits of mass wasting deposits: (i) taluses, (ii) gravitational accumulation deposits and (iii) diamictons. Taluses are generally constituted by granular material not resolvable at the spatial resolution of the chosen NAC images and often show some larger blocks (with diameters ranging from about 2 to 18 m; Pajola et al. 2015) located at the distal part of the deposit. They are uniformly located all along the lower part and at the foot of the walls with rocky appearance, and are therefore, interpreted as the result of a sloping mass of material due to the erosion of adjacent cliffs (Fig. 3d); gravitational accumulation deposits are composed of a material with a wide range of diameters. These deposits are not well sorted and include large boulders (from about 2 to 30 m of diameter; Pajola et al. 2015) supported by fine material-matrix. Their source area is well defined and associated with rough semicircular niches formed for the material detachment from the walls (Fig. 3e); diamicton deposits involve poorly sorted material, as in the case of gravitational accumulation deposits, but, unlike the latter, their source region is not clear (Fig. 3f).

We have also classified different types of lineaments: (i) fractures, (ii) cuesta ridges/terrace margins, (iii) niches and (iv) strata. Fractures are planes along which stress has caused loss of cohesion
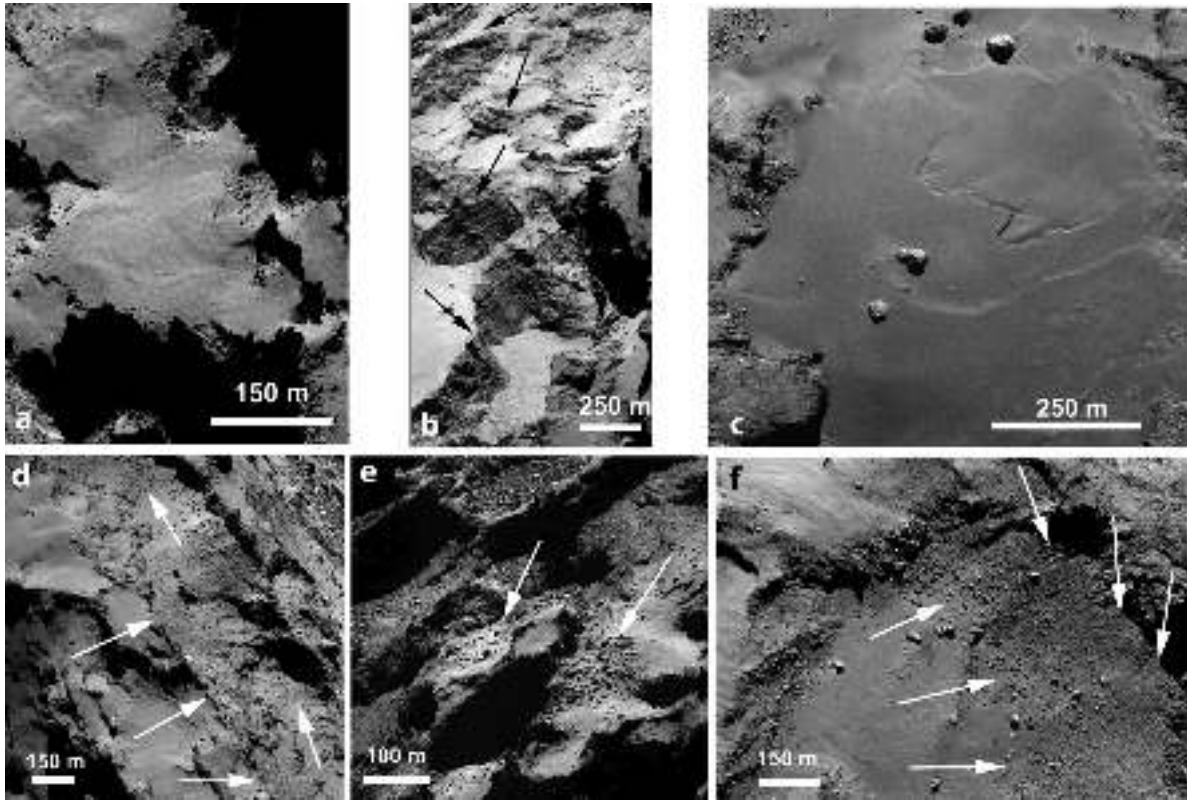
Figure 3. Examples of geologic units identified on the surface of 67P's Northern hemisphere. (a) Fine particle deposits are widespread on the surface. At the OSIRIS resolution they look like a dust mantle. These deposits exhibit localized ripple-like or dune-like features on their surface, likely formed by gas-driven activity. (b) Outcrops of consolidated terrain (indicated by black arrows). This material likely constitutes the bulk of the cometary nucleus; (c) Smooth terrains have been detected in a few areas of the Northern hemisphere surface (the example here is from the Imhotep region). This type of terrain shows a very smooth texture, less rough than the fine particle deposits, suggesting a different formation process for these two materials. Several mass wasting deposits have been identified. These deposits have been subdivided into three subunits: (d) taluses (indicated by white arrows) have been detected all along the feet of high cliffs and exhibit a homogeneous texture, (e) gravitational accumulation deposits are constituted by boulders within a finer matrix, (f) diamicton, deposits with a wide range of granulometry and without a clear source area. In this image the Hatmehit deposits are shown. The source area is unclear since the niches surrounding the deposits are too small to justify the considerable extension of the deposits. Moreover, the largest boulders located at the centre of the depression are very far from the steep walls and therefore can be remnant of collapse and sublimation of a previous superficial area.

in the rock-mass (e.g. Suppe 1985; Fig. 5a). The origin of fractures on 67P is not well defined, although thermal shock and/or thermal fatigue seem to be the most common possible explanation (El-Maarry et al. 2015b; Thomas et al. 2015a). However, for continuous and linear fractures, dynamical stress from collisional events cannot be ruled out (El-Maarry et al. 2015b; Rickman et al. 2015).

Alternative processes, such as tectonic activity due to orbit-/rotation-induced stresses have been proposed (El-Maarry et al. 2015b).

Cuestas are asymmetric ridges showing a steep wall on one side and a gentle dip or back slope on the other (Goudie 2004). They form in the presence of tilted strata where weak strata alternates with harder strata. The latter are less erodible than their weaker counterparts. Differential erosion of these strata creates the typical cuesta landforms which we see on the comet (Fig. 5b; e.g. Simonett 1968; Easterbrook 1999). On 67P, differential erosion by sublimation of strata rich in volatiles, alternated with strata poor in volatile material, which are less erodible, have been invoked to explain these features (La Forgia et al. 2015; Massironi et al. 2015; Pajola et al. 2015). This seems to be supported by the presence of frequent overhangs confining the top of the cuestas' steeper slopes. When the strata are slightly inclined, the differential erosion creates terraces (La Forgia et al. 2015; Massironi et al. 2015; Pajola et al. 2016b).

Therefore, on the geologic maps, we outlined with the same symbol the cuesta ridges, corresponding to the crest of the asymmetric ridges and the terrace margins, which correspond the scarp delimiting the terraces. We use the term 'niches' for the semicircular scarps delimiting the areas of material detachment (Fig. 5c). On 67P, they are often found along cuesta ridges/terrace margins or pits margins.

The linear features classified as 'strata' identify bedding planes which can extend for a few up to hundreds of metres (up to 400 m). They are parallel to each other, usually detected on high walls or scarps and often aligned with well-defined terraces. They also suggest the presence of layered internal structures in 67P's nucleus since they are also observed in the interior walls of pits (Fig. 5d; Massironi et al. 2015).

Mapping both geologic units and lineaments will permit inferences to be made as to the spatial distribution of both. This will shed more light on their origin and, consequently, on the history and evolution of 67P.

3 GEOLOGIC MAPPING PRODUCT

To conveniently cover the entire illuminated surface of the 67P comet nucleus, we generated seven different geologic mapping products: two for the body, two for the head and three for the
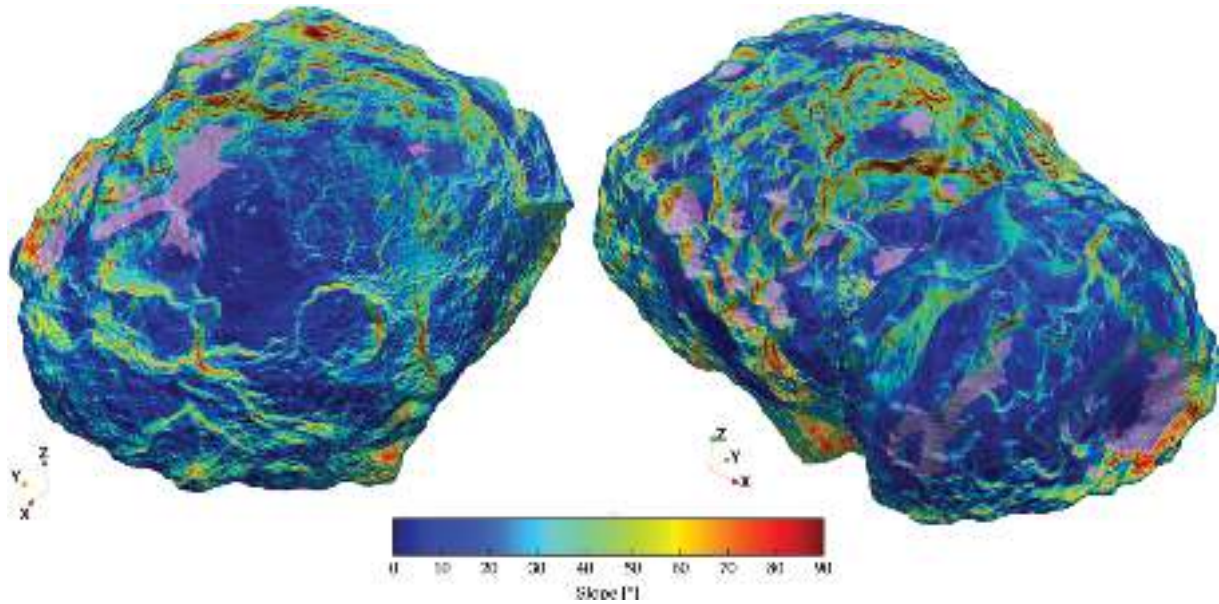
Figure 4. Distribution of mass wasting deposits (areas in pink) detected in the Northern hemisphere. On the background are gravitational slope maps (see the text for more details). Gravitational slopes larger than 90° (overhangs), which constitute only 0.03 per cent of the surface area of the comet, were treated as 90° slopes.
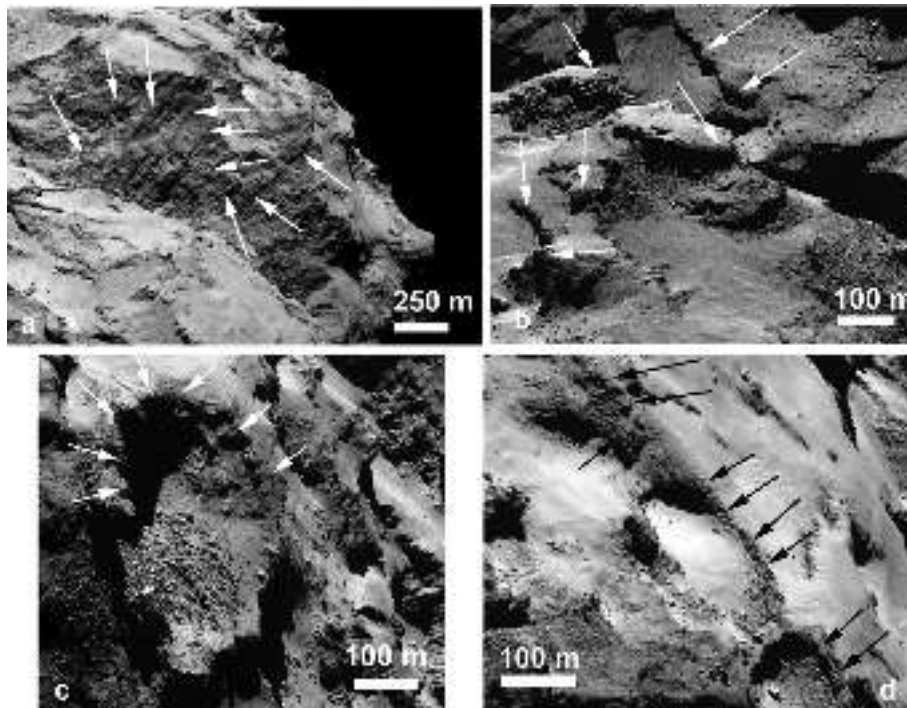
Figure 5. Examples of lineaments detected on 67P's Northern hemisphere. (a) Fractures (indicated by white arrows) detected in the Hathor region; (b) Cuesta ridges (white arrows) formed by differential erosion of a layered terrain (see the text for details); (c) semicircular niche (white arrows) formed by the detachment of material; (d) some strata (black arrows) detected on the larger lobe of the comet.

neck. In this section, we will describe the principal geologic units and linear features detected on each of them.

3.1 Geological mapping of the 'body' of 67P

The body geologic mapping results shown in Figs 6 and 7 highlight the fact that most of the larger lobe's surface, in particular, the Ash,

Aten, Seth, Kephry and Babi physiographic regions, is covered by fine particle deposits (Fig. 8a). The thickness of the deposits appears to be quite variable around the cometary surface. Thomas et al. (2015a,b) noted that these fine particle layers are rather thin at the edges of the mantling deposit but thicker elsewhere. Indeed, such a thickness variability has been observed, for example, in the Ash region, where the fine particle coating on the edge of a pit appears
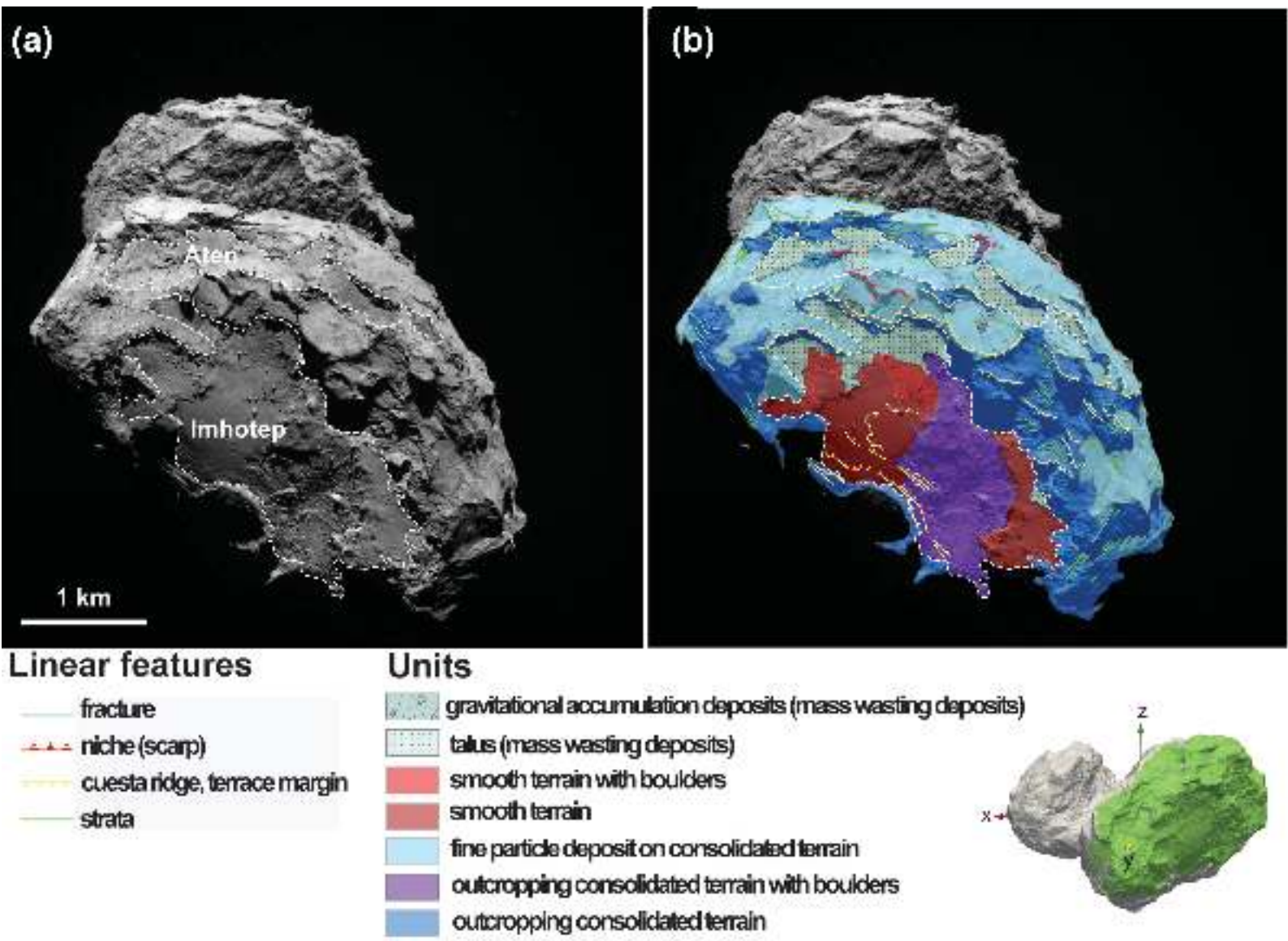
Figure 6. (a) View of the 'bottom side' of the body. (b) Corresponding geologic mapping result. The depressed regions I (Imhotep) and II (Aten) have been outlined with dashed white lines. The legend describes the different lineaments and geologic units detected. For better orientation, the area considered for the mapping has been superposed onto 67P's shape model (Jorda et al. 2016).
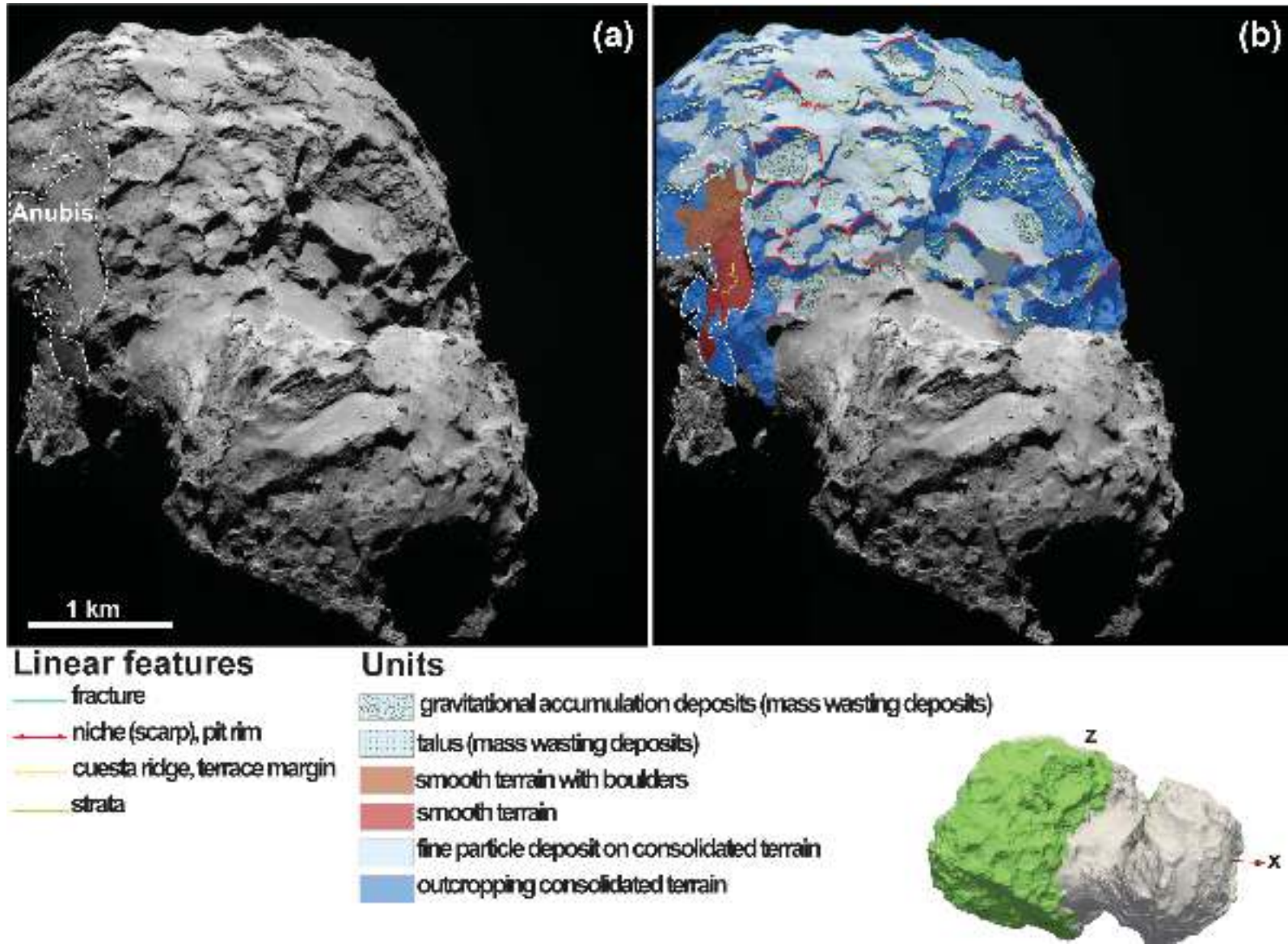
Figure 7. (a) View of the upper side of the body. (b) Corresponding geologic mapping result. The depressed region III (Anubis) has been outlined with dashed white line. The legend describes the different lineaments and geologic units detected. For better orientation, the area considered for the mapping has been superposed onto 67P's shape model.
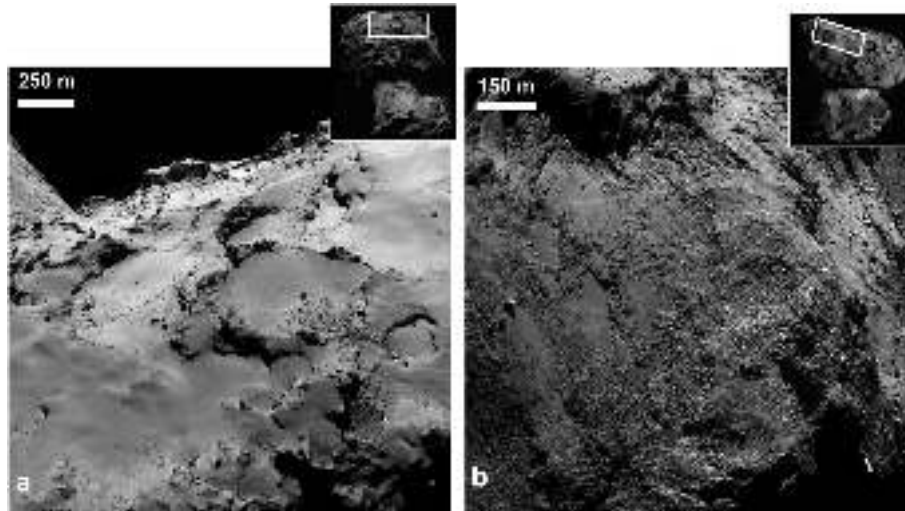
Figure 8. Examples of (a) regions located on the body mantled of fine particle deposits and (b) outcrops of more consolidated material almost free of coating.
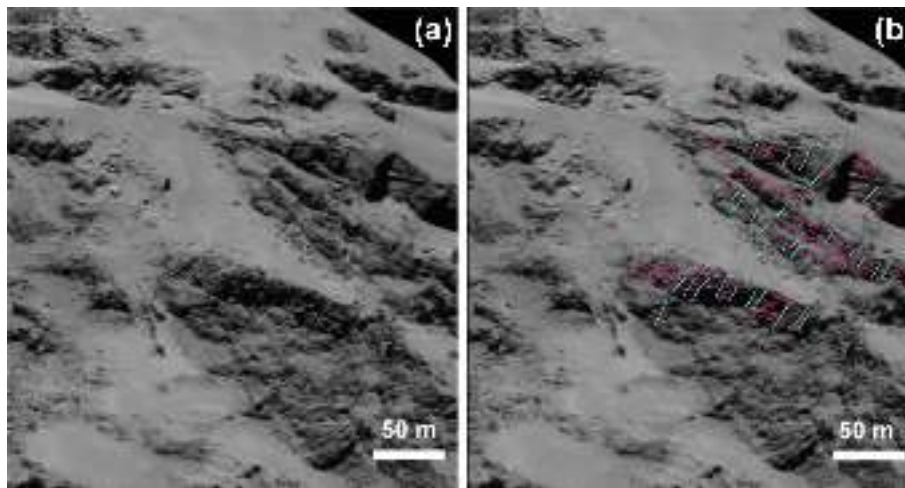
Figure 9. (a) Outcrops of consolidated material. This material shows strata (in pink) and fractures (in cyan). (b) Usually fractures cut strata.

close to the OSIRIS resolution limit (0.34 m pixel^{-1}; Thomas et al. 2015b). On the other hand, a possible 35 m impact crater detected on Ash, suggests that the thickness of fine deposits in some area of the region may reach 1–5 m (El-Maarry et al. 2015a).

Despite the wide spatial cover of the fine deposits on the body, there are some regions which appear almost free of coating and, therefore, it is possible to observe the outcropping of more consolidated material (Fig. 8b). On the body, extended areas of outcropping material are visible in Apis, Atum, Khepry and Aker regions. In other regions, such as Ash, Aten, Seth, Kephry and Babi, the consolidated material is visible in more localized areas, corresponding to areas with the steepest cuesta slopes, cliffs and scarps. The main characteristic of the more consolidated material is the presence of parallel linear features which extend for several metres and are often aligned with terraces. These features were interpreted as strata which reveal the internal stratification of the cometary nucleus (Massironi et al. 2015). Moreover, the consolidated material appears pervaded by randomly oriented fractures, visible both at high and low scale, which attest to the brittle nature of the material. Fractures usually cut the strata head, suggesting that fracturing is younger than the layering (Fig. 9).

One of the most peculiar landforms detected on the body corresponds to the Seth region (Fig. 10), where series of terraces alternate steep walls of outcropping terrains. In several cases, terrace margins exhibit a semicircular shape which could be the result of material collapse which carved out semicircular niches and caused the retreat of the walls (Pajola et al. 2016a).

As a consequence, several deposits of non-sorted material are observed on the terraces at the foot of the cliffs, and are classified as gravitational accumulation deposits. This morphology is most likely due to differential erosion by sublimation of the layers composing the nucleus. Alternatively, Vincent et al. (2015) proposed that at least some of these features represent pits resulting from sinkhole collapse of buried cavities. Most likely though, these semicircular features are the result of the mutual relationship of both processes, acting at different times. Indeed, original collapsed pits can be subjected to differential erosion by sublimation which caused the collapse of material and the retreat of the walls.

For this reason, niches and pit rims on Seth are closely associated with each other and are not clearly discernible. Therefore, they have been outlined with the same symbol in Fig. 7.
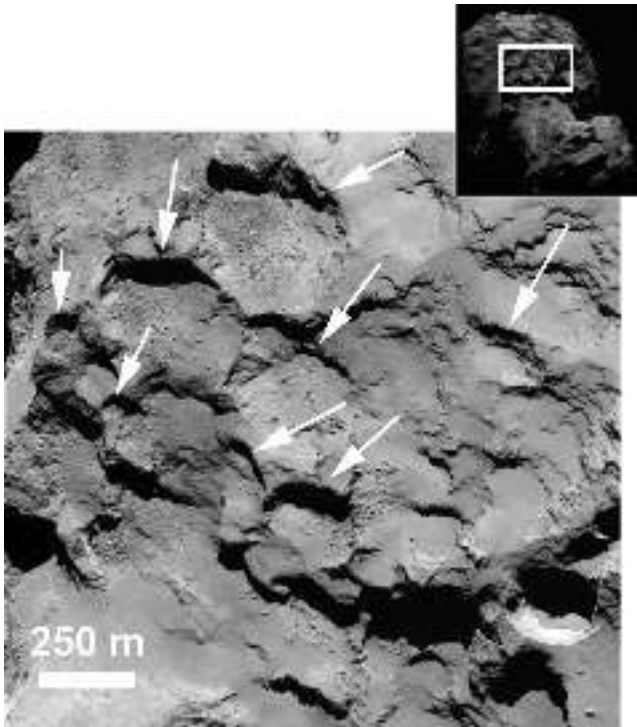
Figure 10. An enlarged view of a section of the Seth region showing particular semicircular features (white arrows) whose origin is linked to erosion processes (see the text for details).

Three large depressed regions have been identified on the body. They have been named Depressed regions I, II and III, corresponding to Imhotep, Aten and Anubis, respectively, following the nomenclature adopted by El-Maarry et al. (2015a; Figs 6 and 7).

3.1.1 Depressed region I (Imhotep)

Imhotep is an extended depression bounded by steep scarps where strata are visible. On the depression floor, we identified a terrain showing a different morphology with respect to the fine material deposits detected outside the depression. This suggests that a material with different properties is present here and we mapped it as smooth terrain unit. Boulders are nearly absent at the centre of the depression whereas their number sensibly increases near the edges. At the interface between Kepry and Imhotep several taluses are observed and mapped accordingly. The distribution and extension of outcropping terrain and smooth terrain on the resulting Imhotep geological map is in accordance with the previous map of Auger et al. (2015) of the same region. However, the map presented here also takes into account the mass wasting deposits, whereas in the Auger et al. (2015) work the distribution and size of boulders have been highlighted more.

The thickness of the smooth terrain is variable and decreases gradually revealing the underlying rocky terrain (Auger et al. 2015). This terrain seems to be composed of consolidated materials characterized by rougher textures and is heavily affected by fractures. A large number of boulders, with a great variety of dimensions, are observed in this consolidated terrain. Both smooth and rocky terrains display terraces (Fig. 6). Some of them cross the rocky/smooth terrain boundary showing no discontinuities, suggesting a continuity of the rocky terrain topography under the smooth material

(Auger et al. 2015) and the presence of a consolidated stratified substratum underneath the smooth deposits.

3.1.2 Depressed region II (Aten)

Close to Imhotep is Aten, an elongated, irregular, deep depression almost entirely filled by fine particle deposits locally covered by taluses. Outcropping of consolidated material is rare and is detected only on the margin of the depression in correspondence with the steep walls (Fig. 6).

3.1.3 Depressed region III (Anubis)

The third depression detected on the body corresponds to Anubis. From a morphological point of view, it resembles the Imhotep region. Indeed, the depression floor is filled in the central areas with smooth terrain, although less extended than that of Imhotep, surrounded by a rougher terrain rich in boulders. Several buried terraces have been detected in this depression and all are in areas with smooth terrain (Fig. 7), suggesting a stratified substratum.
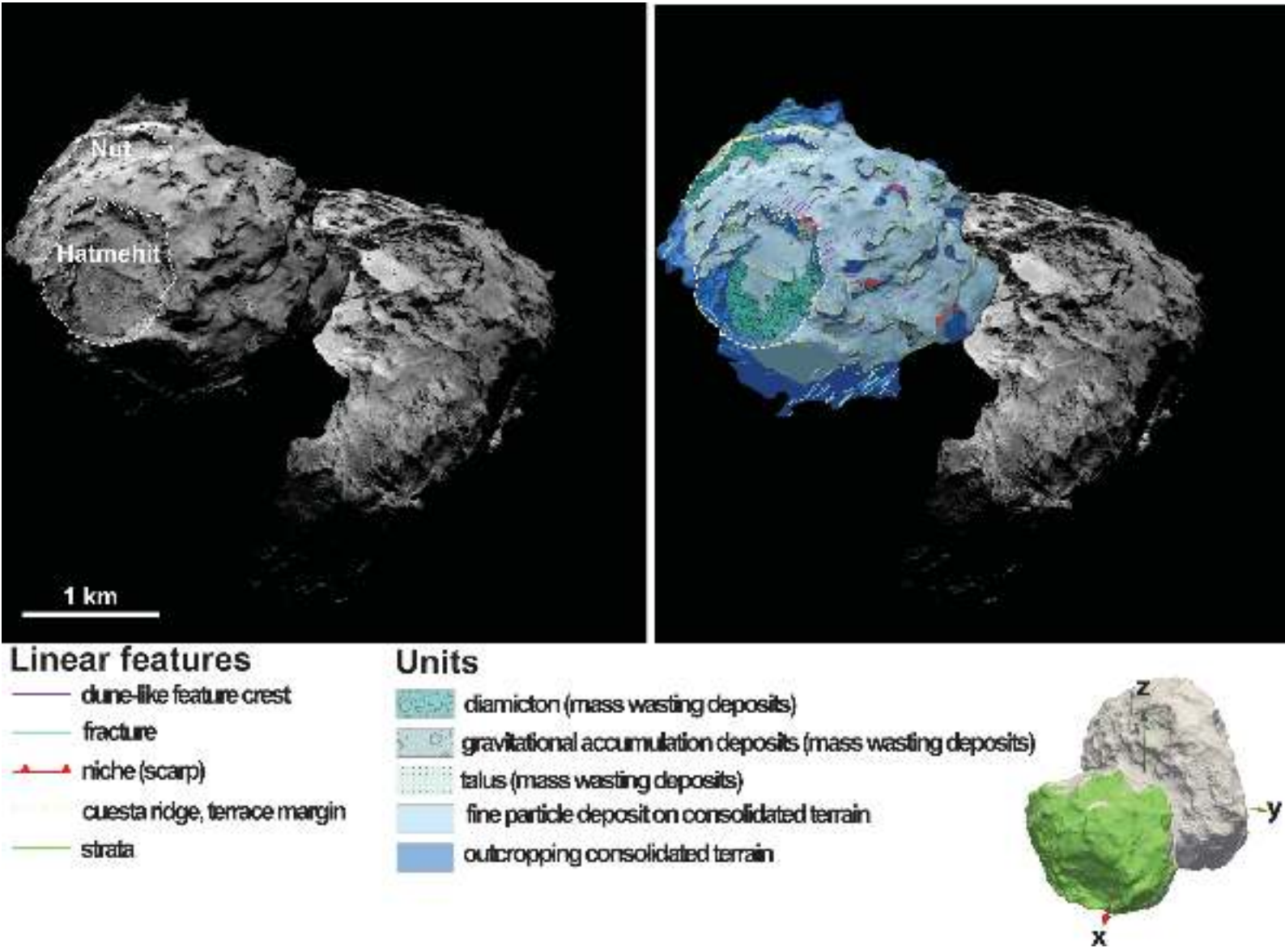
3.2 Geologic mapping of the 'head' of 67P

Similar to the body, results from the mapping of the head shown in Figs 11 and 12 reveal that the minor lobe is dominated by fine particle deposits (Fig. 13a). In particular, Ma'at, Nut, and a great part of Maftet are coated with these deposits. Locally, fine dusty particle deposits show several dune-like forms (Fig. 14). These features resemble terrestrial linear dunes which form when wind blows from more than one directions, although one direction must predominate. The longest axes of the dunes are parallel to the dominant wind direction (e.g. Melosh 2011). In the case of 67P, the process proposed to explain these dune-like forms is wind linked to outburst activity (Thomas et al. 2015a,b). This type of feature is particularly evident on Ma'at, Hatmehit and Nut, where dune-like forms are arranged in fields. Interestingly, for the most part log axes of the features are iso-oriented, suggesting that, if these features are effectively created by gas-driven wind, the predominant wind direction is constant through all of these regions (La Forgia et al. 2015). At a submetre-scale resolution, some of the dunes-like features near the rim of the Hatmehit depression, particularly those located on the Ma'at and Maftet regions, show chains of pit-like features whose origin can be related to wind erosion or sublimation processes (Fig. 14b; La Forgia et al. 2015; Thomas et al. 2015b).

On the fine deposit-covered areas, widespread outcrops of more consolidated material have been detected in correspondence with the location of cuestas. At the foot of the cliff, taluses or gravitational accumulation deposits have been repeatedly identified. Extended outcropping of consolidated material corresponds to Anuket regions, where strata are well discernible, as well as several small terraces (Fig. 13b; Massironi et al. 2015). However, the most outstanding region of outcropping material on the lobe is represented by the Hathor region, which presents a view into the head's internal structure (Fig. 11). This region is an outcrop of about 900 m in height and 1500 m in width (Massironi et al. 2015; Rickman et al. 2015) where a huge amount of strata, regular and parallel to each other, have been detected extending for several hundreds of metres. Usually, layers are cross-cut by fractures which show a uniform perpendicular trend. On both sides of Hathor, the layering changes orientation, whereas at the boundary between Hathor and Ma'at no significant change has been detected (Fig. 11).
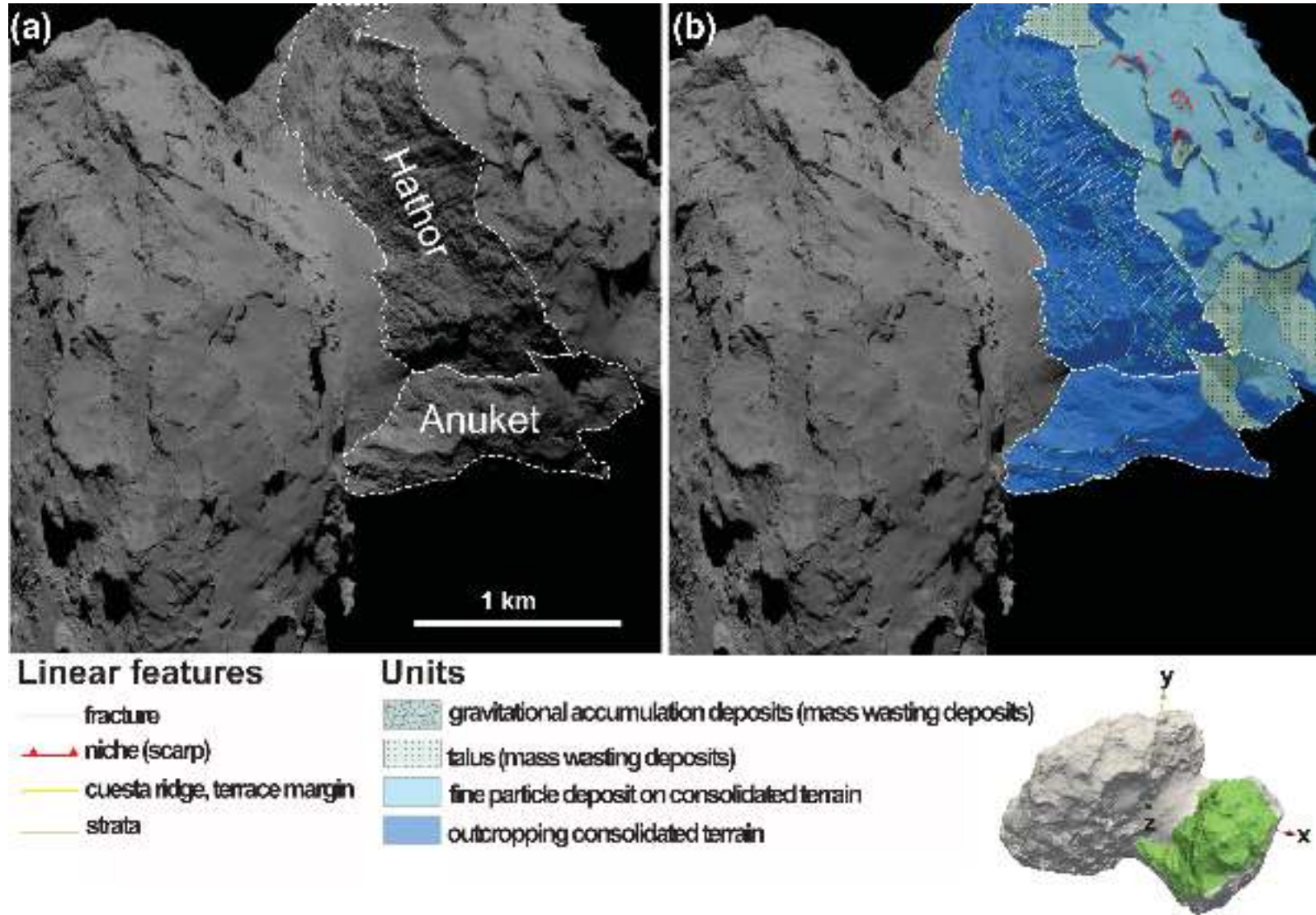
Figure 11. (a) View of the bottom side of the head and (b) its corresponding geologic mapping result. Hathor and Anuket areas have been outlined with dashed white lines. The legend describes the different lineaments and geologic units detected. For better orientation, the area considered for the mapping has been superposed onto 67P's shape model.
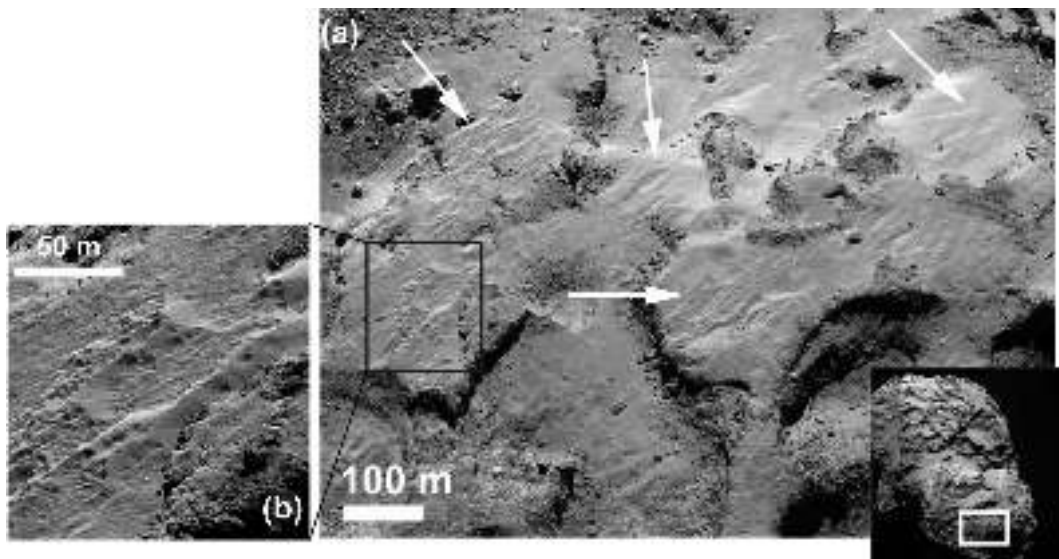
Linear features

— dune-like feature crest
— fracture
▲—▲ niche (scarp)
— cuesta ridge, terrace margin
— strata

Units

diamicton (mass wasting deposits)
gravitational accumulation deposits (mass wasting deposits)
talus (mass wasting deposits)
fine particle deposit on consolidated terrain
outcropping consolidated terrain

Figure 12. (a) View of the upper side of the head and (b) its geomomorphological interpretation. The depressed regions IV (Nut) and V (Hatmehit) have been outlined with dashed white lines. The legend describes the different lineaments and geologic units detected. For better orientation, the area considered for the mapping has been superposed onto 67P's shape model.
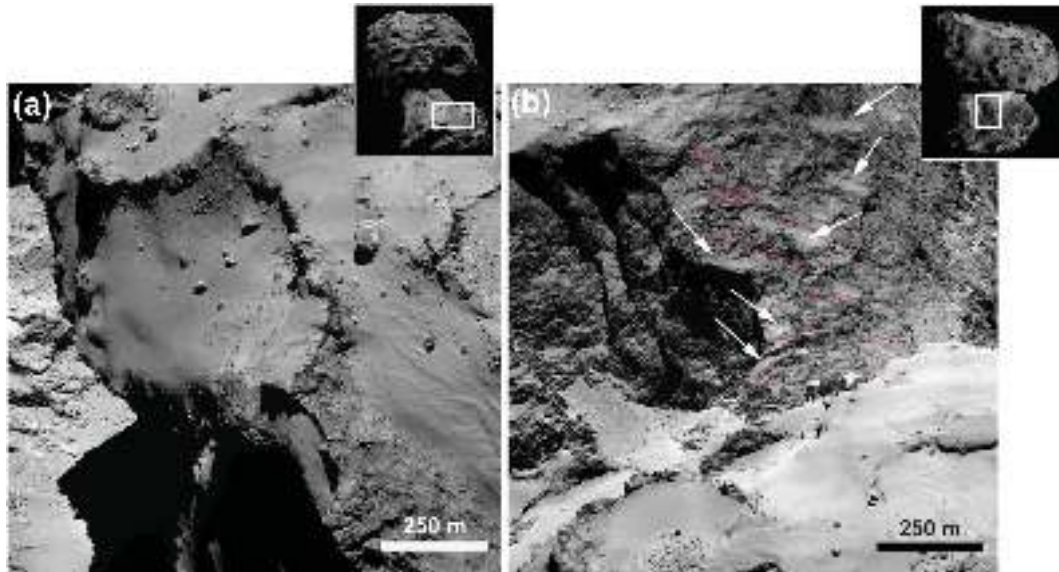
Figure 13. Examples of (a) a region, located on the head, covered by fine particle deposits (b) and a region of outcropping consolidated material. Pink lines on (b) indicate some strata heads, whereas white arrows indicate small aligned terraces (see also Massironi et al. 2015).

Figure 14. (a) View of linear features detected on the head, near the Hatmehit depression, and interpreted to be dune-like features (indicated by white arrows). In this region, some of these dune-like features show chains of pits (b), likely formed by wind erosion or sublimation processes.

This observation led Massironi et al. (2015) to suggest that Hathor represents the internal structures of Anuket. Moreover, Thomas et al. (2015a) highlighted how Anuket seems to extend underneath the Ma'at region. Another region almost free of dust is represented by Bastet, which is partially visible since it extends into the non-illuminated areas (Fig. 15). Bastet shows clear terraces but not outcrops with pervasive layering, beside the boundary with Hathor, where some strata have been mapped. Bastet region appears heavily fractured with iso-oriented fractures which seem to form a system and which are occasionally cross-cut by other fractures with different orientation (El-Maarry et al. 2015a; La Forgia et al. 2015). Also, similarly to the body, depressed regions have been detected on the head of the comet (Fig. 12). These depressed regions have been numbered as IV and V, corresponding to the Nut and Hatmehit regions, respectively (El-Maarry et al. 2015a).

3.2.1 Depressed region IV (Nut)

This lowland resembles a large denudation terrace covered by deposits of fine particles overlaid by a poorly sorted diamicton deposit (Fig. 12). The presence of these deposits does not allow the detection of outcropping material.

3.2.2 Depressed region V (Hatmehit)

One of the most peculiar depressions is located on the distal part of the head, and corresponds to the Hatmehit region (Fig. 12). It is represented by a rather circular depression bounded by steep walls, the highest reaching 150 m, showing strata. Along the rim of this depression, several centripetally arranged terraces have been detected. These terraces are probably the result of differential erosions of slightly inclined strata. Locally, steep walls appear to have
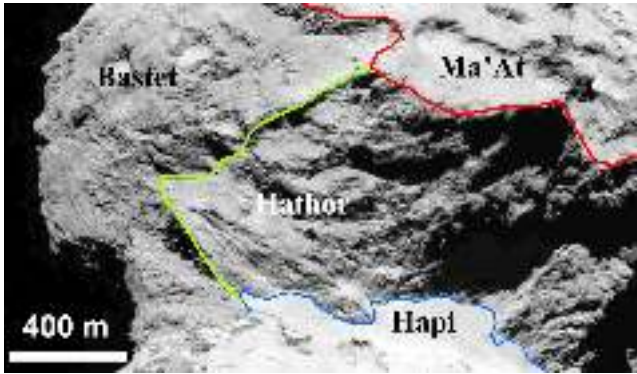
Figure 15. View of Bastet region and surrounding physiographic areas. Bastet corresponds to an extended outcrop of consolidated material. The red line indicates the boundary with the Ma'at region, the green line the boundary with Hathor and the blue line highlights the boundary with the Hapi region.

collapsed forming taluses and gravitational accumulation deposits and creating some semicircular niches. The floor of Hatmehit is rather flat and partially covered by diamicton (Fig. 12). The possible origin of the deposits is not clear. The incoherent material deposited near the margin could have formed by the erosion of the walls (La Forgia et al. 2015); however, the very small niches detected can hardly justify the detachment of the great amount of deposits observed. Moreover, the boulders present at the centre of the depression, far from the surrounding steep walls, could be the remnants of a past superficial area collapsing and sublimating (Pajola et al. 2015).

3.3 Geologic mapping of the 'neck' of 67P

One of the connecting areas between the two lobes, corresponding to the Hapi region, is covered by fine particle deposits (Fig. 16). Locally, several dune-like features have been observed (Fig. 17a). They resemble terrestrial longitudinal dunes and have their longest axes roughly aligned to E–W and are arranged in a field (Thomas et al. 2015b). At the centre of Hapi is a row of large boulders, which are probably blocks detached from the adjacent Hathor outcrop (Pajola et al. 2015).

Several taluses have been also observed, which probably originated from the adjacent cliffs of Seth and Aker, on one side, and Hathor, Anuket and Bastet, on the other. Very small areas of outcropping of more consolidated material have been observed. These outcrops show few strata whose orientation varies throughout the neck. For instance, at the centre of the neck (Fig. 16b), stratum orientation seems coherent with that of Seth, whereas on the facing zone of Anuket and Seth (Fig. 16d), the orientation is consistent with that of Anuket.

Moreover, a crack, of about 440 m in length, has been detected in proximity of Hathor. This lineament seems to be constituted by aligned pits, which can be the result of dilatational stress or hybrid fracturing (Ferrill et al. 2004; Wyrick et al. 2004), or could be formed by sublimation-induced torques (Hirabayashi et al. 2016; Fig. 17b).

4 DISCUSSION AND CONCLUSIONS

In this work, we presented the geologic maps of the 70 per cent of Churyumov–Gerasimenko nucleus surface (corresponding to the il-

luminated area during 2014 August–September). The work includes two maps of the head, two of the body and three of the neck. These maps are the first geologic maps of 67P's Northern hemisphere and group surface areas with similar morphological, textural and stratigraphic characteristics into the same unit. We identified four main geologic units: (i) fine particle deposits, (ii) consolidated material, (iii) smooth terrain and (iv) mass wasting deposits. On the basis of their granulometry and source of origin, these deposits have been further classified as taluses, gravitational accumulation deposits or diamictons. Also, linear features have been mapped and grouped into five main categories: (i) fractures, (ii) strata, (iii) cuesta ridges and terrace margins, (iv) niches and (v) dune-like feature crests.

This *geologic* mapping approach has never been performed before on the nucleus of 67P, except in a few, very specific locations (i.e. Philae landing site, by La Forgia et al. 2015; Imhotep region, by Auger et al. 2015; and Answan region, by Pajola et al. 2016a). The other available global maps of 67P nucleus are *physiographic* maps (i.e. El-Maarry et al. 2015a), which specifically classify the comet nucleus surface into different broad regions, taking into account mainly geographical and topographic boundaries. Therefore, in that case no geomorphologic characteristics of the surface (texture, granulometry, forms, origin source of deposits), as well as linear features, were taken into account.

The extension and geographical distribution of the geologic units on the surface are of paramount importance on improving the knowledge of cometary nuclei and its thermophysical characteristics. Indeed, the geologic maps allow the distinction of surfaces of different nature such as the consolidated material, constituting the bulk of the 67P nucleus and the incoherent materials mantling its surface. Surface roughness, particle size, exposure of solid rocks and boulders, taken into account in the geologic mapping, are all factors which influence the surface thermal inertia (e.g. Mellon et al. 2000; Delbo et al. 2007; Davidsson et al. 2013).

The geologic maps presented showed that the fine particles deposits are the most extensive geologic unit in the Northern hemisphere. Indeed, they are widespread on both nucleus' lobes and cover almost the entire neck. This distribution can be explained as the result of airfalls, i.e. particles ejected by rapidly expanding gases which have not enough energy to escape the comet, and that deposited over much of the Northern hemisphere (Thomas et al. 2015b). Spectroscopic analysis by VIRTIS (Visible and Infrared Thermal Imaging Spectrometer; Coradini et al. 2007) suggests that the mantling material is composed of opaque minerals associated with non-volatile organic material (Capaccioni et al. 2015).

Outcropping of more consolidated material is the second most common geologic unit: it is easily visible in the region free of dust deposits, while in the area covered by fine deposits it is evident only in association with cliffs. Outcrops allow us to observe the material which likely constitutes the bulk of 67P's nucleus. The numerous mapped fractures reveal the brittle nature of the material. The formation process for this terrain is still unclear. We know that the porosity of the nucleus is very high (about 70–80 per cent), and that the density is estimated to be 533 ± 6 kg m^{-3} (Pätzold et al. 2016). Spectrophotometric analyses performed with NAC images, coupled with laboratory experiments, are compatible with the presence of an uppermost dark mantle of refractory dust which overlies an ice-rich subsurface (Pommerol et al. 2015; Filacchione et al. 2016). Metre-scale exposures of this ice-rich material have been detected as bright spots on the surface of some boulders and in some outcrops (Pommerol et al. 2015; Filacchione et al. 2016).

Interestingly, in correspondence with outcrops several strata have been mapped giving evidence of stratification, which offers
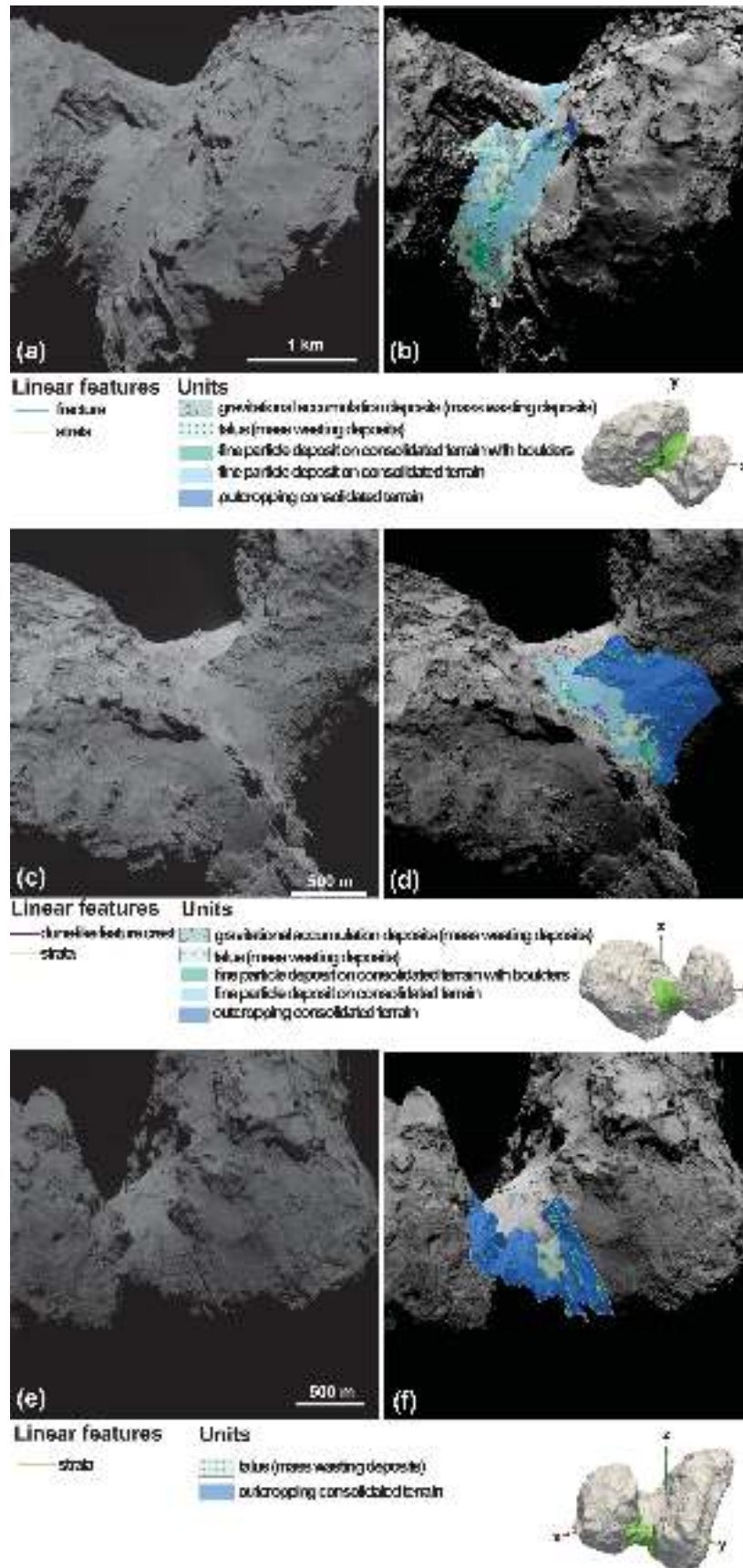
Figure 16. (a), (c) and (e) Three views of the neck region from different perspectives and (b), (d) and (f) their corresponding geologic mapping interpretations. Legend describes the different lineaments and geologic units detected. For better orientation, the areas considered for the mapping have been superimposed onto 67P's shape model.
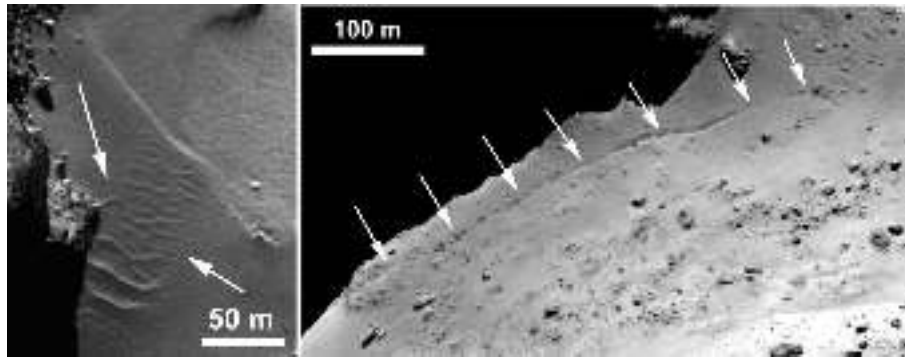
Figure 17. Examples of features detected on the neck. (a) Enlarged view showing a field of iso-oriented dune-like forms. (b) Enlarged view of an ∼440-m-long crack detected on the neck region (indicated by white arrows). This fracture seems to be constituted of aligned pits.

important clues regarding the origin of the comet. The most impressive outcropping area is the Hathor region. This is the most extended outcropping terrain of the entire nucleus showing tens of strata and terraces.

Evidence of layering was already detected on other cometary nuclei, such as that of 9P/Tempel 1 (Thomas et al. 2007) and likely of 81P/Wild 2 (Brownlee et al. 2004) and 19P/Borrelly (Britt et al. 2004). Different hypotheses have been proposed to explain this phenomenon, such as (i) deposition of lag material (Basilevsky & Keller 2006) (ii) flow of fluidized material (Belton & Melosh 2009), (iii) radially symmetric thermal processes of an originally homogeneous body (Thomas et al. 2007) or (iv) a primordial accretion leading to an inner-layered structure (Belton et al. 2007; Lasue et al. 2009). For 67P's layered nucleus, a primordial stratification has been suggested by Massironi et al. (2015). In addition, by gravitational considerations and geologic sections, which reconstruct the geological structure of the interior of the nucleus, they proposed that both lobes have a distinct onion-like stratification and, therefore, that they are likely the result of two independently formed objects before merging into a single bilobed nucleus.

Another frequent geologic unit mapped on 67P's Northern hemisphere is represented by gravitational deposits, which have been observed for the first time on a comet. The geologic maps highlight that these deposits are scattered all over the surface, as inferred by the large number of taluses, gravitational deposit accumulations and diamictons detected in numerous areas on the cometary surface. This would further support the hypothesis that the material constituting the nucleus is susceptible to fracturing, differential erosion by sublimation and gravitational collapse.

The fine smooth terrains are less frequent. They are localized inside the most extended depressions of the body (i.e. Imhotep and Anubis) and are constituted by fine material characterized by a smoother texture with respect to that of fine particle deposits, suggesting a different origin for these two types of unit. However, the origin of these smooth terrains is still debated. Auger et al. (2015) suggested three possible origins: (i) it can be formed in situ, (ii) it can be composed of deposits collapsed form the scarps edging the depression or (iii) it can be airfall deposits.

The distinction of this great variability of geologic units on the comet nucleus will help in addressing a detailed spectral/compositional analysis of the different kinds of material located on the surface. This will help with better understanding the spectral variegation of the surface and attributing a characteristic spectral behaviour to each unit, contributing to better knowledge of their formation and origin.

Extended depressed regions are not rare on the nucleus and are observed both on the head and body. These features can give important information on the evolution of the comet. Indeed, they suggest that the activity of the comet could have been high enough to eject great amounts of material or to cause partial collapse in some regions. These processes are the most probable candidate for forming the Aten depression, located on the body, which likely formed from the collapse of the surface and the subsequent retiring of the walls by erosion due to sublimation (Thomas et al. 2015a). Signs of erosion, likely due to outgassing activity, have also been registered on the Imhotep depression, where several new scarps have been observed to develop through time in correspondence of the location of smooth terrains (Groussin et al. 2015b).

One of the depressions, corresponding to Hatmehit region, is circular in shape. Its origin is still debated, since its shape resembles the circular depressions attributed to impacts observed on 81P/Wild 2 (Brownlee et al. 2004). However, an impact origin seems unlikely due to its morphology, coherent centripetally arranged terraces observed on its margins, and the long terrace crossing its floor, which do not fit with the expected morphology of an impact crater on a layered terrain (La Forgia et al. 2015). A possible formation process, proposed by Pajola et al. (2015), involves the collapse of terrain due to sublimation of an underlying volatile-rich stratum.

Finally, one of the most remarkable landforms of 67P is the semi-circular features observed on Seth, where the mapping highlighted a complex interconnection between linear features and geomorphologic units. Indeed, terraces alternate with steep walls showing outcrops of more consolidated material. These forms are likely the expression of the evolution of pits, formed through the collapse of buried cavities, whose shape was modified afterwards due to sublimation which caused the progressive erosion, and the consequent retreat, of the walls. This is indicated by the gravitational accumulation deposits detected at the foot of the walls (Pajola et al. 2015; Vincent et al. 2016).

Geologic mapping of comet 67P's Northern hemisphere highlights the complex and the extremely variable textures and features characterizing its surface. By comparing our maps with those of the Southern hemisphere presented in Lee et al. (2016), we observed that the most predominant difference is the paucity of fine particle deposits on the southern regions, with the consequent prevalence of areas of outcropping consolidated terrain (Lee et al. 2016). This is likely due to the different insolation condition of the two hemispheres (Groussin et al. 2015b; Keller et al. 2015; Lee et al. 2016).

As expected for comets, 67P/Churyumov–Gerasimenko's shape and surface morphology have been, and will continue to be,

modified during its evolution. Therefore, the geomorphologic mapping products can be a useful tool as reference maps, in order to better highlight and discern the transformations of its surface.

REFERENCES

A'Hearn M. F. et al., 2005, Science, 310, 258
A'Hearn M. F. et al., 2011, Science, 332, 1396
Auger A.-T. et al., 2015, A&A, 583, A35
Basilevsky A. T., Keller H. U., 2006, Planet. Space Sci., 54, 808
Belton M. J. S., Melosh J., 2009, Icarus, 200, 280
Belton M. J. S. et al., 2007, Icarus, 187, 332
Britt D. T. et al., 2004, Icarus, 167, 45
Brownlee D. E. et al., 2004, Science, 304, 1764
Capaccioni F. et al., 2015, Science, 347, aaa0628
Coradini A. et al., 2007, Space. Sci. Rev., 128, 529
Davidsson B. J. R. et al., 2013, Icarus, 224, 154
Delbo M., dell'Oro A., Harris A. W., Mottola S., Mueller M., 2007, Icarus, 190, 236
Easterbrook D. J., 1999, Surface Processes and Landforms, 2nd edn. Prentice-Hall, Upper Saddle River, NJ
El-Maarry M. R. et al., 2015a, A&A, 583, A26
El-Maarry M. R. et al., 2015b, Geophys. Res. Lett., 42, 5170
Ferrill D. A., Wyrick D. Y., Morris A. P., Sims D. W., Franklin N. M., 2004, GSA Today, 14, 4
Filacchione G. et al., 2016, Icarus, 274, 334
Goudie A., 2004, Encyclopedia of Geomorphology. Routledge, London
Groussin O. et al., 2015a, A&A, 583, A32
Groussin O. et al., 2015b, A&A, 583, A36
Hirabayashi M. et al., 2016, Nature, 534, 352
Jorda L., Lamy P. L., Gaskell R. W., Kaasalainen M., Groussin O., Besse S., Faury G., 2012, Icarus, 221, 1089
Jorda L. et al., 2016, Icarus, 277, 257
Keller H. U. et al., 2007, Space Sci. Rev., 128, 433
Keller H. U. et al., 2015, A&A, 583, A34
LaForgia F. et al., 2015, A&A, 583, A41
Lasue J., Botet R., Levasseur-Regourd A. C., Hadamcik E., 2009, Icarus, 203, 599
Lee J.-C. et al., 2016, MNRAS, in press
Massironi M. et al., 2015, Nature, 526, 402

Mellon M. T., Jakosky B. M., Kieffer H. H., Christensen P. R., 2000, Icarus, 148, 437
Melosh H. J., 2011, Planetary Surface Processes. Cambridge Univ. Press, Cambridge
Mottola S. et al., 2014, A&A, 569, L2
Mottola S. et al., 2015, LPI Contrib., 1832, 2308
Pajola M. et al., 2015, A&A, 583, A37
Pajola M. et al., 2016a, A&A, 592, A69
Pajola M. et al., 2016b, MNRAS, 462, S242
Pätzold M. et al., 2016, Nature, 530, 63
Pommerol A. et al., 2015, A&A, 583, A25
Rickman H. et al., 2015, A&A, 583, A44
Sierks H. et al., 2015, Science, 347, 1044
Simonett D. S., 1968, in Fairbridge R. W., ed., Encyclopedia of Geomorphology. Reinhold, New York, p. 1233
Suppe J., 1985, Principles of Structural Geology. Prentice-Hall, Englewood Cliffs, NJ, p. 537
Tanaka K. L., Skinner J. A., Jr, Hare T. M., 2011, Planetary Geologic Mapping Handbook – 2011. Abstracts of the Annual Meeting of Planetary Geologic Mappers. NASA Goddard Space Flight Center, Greenbelt, MD
Thomas P. C. et al., 2007, Icarus, 187, 4
Thomas P. C. et al., 2013, Icarus, 222, 453
Thomas N. et al., 2015a, Science, 347, 04401
Thomas N. et al., 2015b, A&A, 583, A17
Tubiana C. et al., 2015, A&A, 583, A46
Vincent J.-B. et al., 2015, Nature, 523, 63
Vincent J.-B. et al., 2016, A&A, 587, A14
Werner R. A., Scheeres D. J. 1996, Celest. Mech. Dyn. Astron., 65, 313
Wyrick D. Y., Ferrill D. A., Morris A. P., Colton S. L., Sims D. W., 2004, J. Geophys. Res., 109, E06005

[1]*Dipartimento di Geoscienze, University of Padova, via G. Gradenigo 6, I-35131 Padova, Italy*
[2]*Physikalisches Institut der Universität Bern, Sidlerstr. 5, CH-3012 Bern, Switzerland*
[3]*Center of Studies and Activities for Space (CISAS) 'G. Colombo', University of Padova, Via Venezia 15, I-35131 Padova, Italy*
[4]*NASA Ames Research Center, Moffett Field, CA 94035, USA*
[5]*School of Physical Sciences, The University of Kent, Canterbury, Kent, CT2 7NZ, UK*
[6]*Dipartimento di Fisica e Astronomia 'G. Galilei', University of Padova, vic. Osservatorio 3, I-35122 Padova, Italy*
[7]*INAF Osservatorio Astronomico di Padova, vic. dell'Osservatorio 5, I-35122 Padova, Italy*
[8]*Department of Information Engineering, University of Padova, via Gradenigo 6/B, I-35131 Padova, Italy*
[9]*Max-Planck-Institut für Sonnensystemforschung, Justus-von-Liebig-Weg 3, D-37077 Göttingen, Germany*
[10]*Laboratoire d'Astrophysique de Marseille, UMR 7236, CNRS & Aix-Marseille Université, 38 rue Frédéric Joliot-Curie, F-13388 Marseille cedex 13, France*
[11]*Centro de Astrobiología, CSIC-INTA, Torrejón de Ardoz, E-28850 Madrid, Spain*
[12]*International Space Science Institute, Hallerstraße 6, CH-3012 Bern, Switzerland*
[13]*PAS Space Research Centre, Bartycka 18A, PL-00716 Warszawa, Poland*
[14]*Department of Physics and Astronomy, Uppsala University, Box 516, SE-75120 Uppsala, Sweden*
[15]*Scientific Support Office, European Space Research and Technology Centre/ESA, Keplerlaan 1, Postbus 299, NL-2201 AZ Noordwijk ZH, the Netherlands*
[16]*Institut für Geophysik und extraterrestrische Physik, TU Braunschweig, D-38106 Braunschweig, German*
[17]*Department of Astronomy, University of Maryland, College Park, MD 20742-2421, USA*
[18]*LESIA-Observatoire de Paris, CNRS, UPMC, Univ. Paris 06, Univ. Paris-Diderot, 5 Place J. Janssen, F-92195 Meudon Principal Cedex, France*

[19]*LATMOS, CNRS/UVSQ/IPSL, 11 Boulevard d'Alembert, F-78280 Guyancourt, France*

[20]*CNR-IFN UOS Padova LUXOR, via Trasea 7, I-35131 Padova, Italy*

[21]*University of Trento, via Sommarive 9, I-38123 Trento, Italy*

[22]*Department of Industrial Engineering, University of Padova, Via Venezia 1, I-35131 Padova, Italy*

[23]*Univ. Paris Diderot, Sorbonne Paris Cité, 4 Rue Elsa Morante, F-75205 Paris Cadex 13, France*

[24]*INAF Osservatorio Astronomico di Trieste, Via Tiepolo 11, I-34014 Trieste, Italy*

[25]*Instituto de Astrofísica de Andalucía-CSIC, E-18008 Granada, Spain*

[26]*Deutsches Zentrum für Luft- und Raumfahrt, Institut für Planetenforschung, Rutherfordstraße 2, D-12489 Berlin, Germany*

[27]*Graduate Institute of Astronomy, National Central University, 300 Chung-Da Rd Chung-Li 32054, Taiwan*

[28]*Operations Department European Space Astronomy Centre/ESA, P.O. Box 78, E-28691 Villanueva de la Cañada, Madrid, Spain*

[29]*Institut für Datentechnik und Kommunikationsnetze der TU Braunschweig, Hans-Sommer-Str. 66, D-38106 Braunschweig, Germany*

This paper has been typeset from a TeX/LaTeX file prepared by the author.